

Long-Term Measurements of NO₃ Radical at a Semiarid Urban Site: 2. Seasonal Trends and Loss Mechanisms

DAVID ASAF,* ERAN TAS,
DANIEL PEDERSEN, MORDECHAI PELEG,
AND MENACHEM LURIA

*Institute of Earth Sciences, The Hebrew University of
Jerusalem, Edmud-Safra Campus, Givat-Ram, Israel*

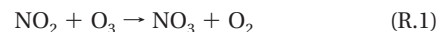
*Received March 26, 2010. Revised manuscript received
June 4, 2010. Accepted June 17, 2010.*

This study is the first to present long-term measurements of the nitrate radical in an urban location. Extensive nitrate radical measurements were conducted together with ancillary parameters during a continuous two year campaign (2005–2007) in the semiarid location of Jerusalem. The average nighttime NO₃ concentration was 27.3 ± 43.5 ppt, the highest ever reported, with a seasonal average peak during summer (33.3 ± 55.8 pptv) with maximum levels exceeding 800 pptv. Significant diurnal changes in NO₃ concentrations were observed, caused by an unusual nighttime increase in ozone concentrations. The NO₃ loss processes exhibited strong seasonal variability. Homogeneous gas-phase losses were the main removal processes during summer and spring. The heterogeneous losses of N₂O₅, averaged over the entire campaign, contributed to less than half of the direct losses even though they dominated the winter seasons and part of the autumn months. Statistical regression analysis showed that NO₃ was inversely correlated with relative humidity and positively correlated with temperature and to a lesser extent with NO₂ and O₃, indicating that the heterogeneous removal processes were also important. The diurnal behavior of NO₃ was examined using a one-dimensional chemical transport model. The simulations showed that NO₃ trends and concentrations were influenced mainly by changes in ozone and nitrogen oxide levels and that the very high levels of NO₃ can be explained by the entrainment of fresh ozone from the upper atmospheric levels. After sunset and in the early morning, the homogeneous processes are the major loss pathways, while the heterogeneous N₂O₅ removal pathway dominates the intermediate times.

1. Introduction

Nitrate radicals (NO₃) play a major role in the nocturnal atmosphere. Characterizing the diurnal and seasonal variability of its behavior is of particular importance for understanding nighttime chemical mechanisms. The importance of NO₃ as an atmospheric oxidant, and as a sink for nitrogen oxides and volatile organic compounds (VOCs), has been well established and reported in previous papers (1–4) and is presented briefly below.

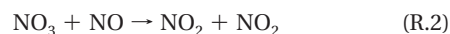
The major source of NO₃ in the boundary layer is the reaction of NO₂ with O₃ (R.1)



The production rate of NO₃ {P_{NO₃}} by this reaction is given in refs 5, 6

$$P_{\text{NO}_3} = k_1[\text{NO}_2][\text{O}_3] \quad (1)$$

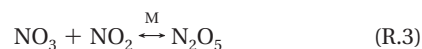
NO₃ has limited oxidative capacity during daytime due to its rapid photolysis and rapid gas-phase reaction with NO (R.2), thus preventing its accumulation and leading to a lifetime of less than 1 s.



Nocturnal NO concentrations are usually low due to limited fresh emissions and rapid oxidation with ozone. Nevertheless in polluted urban areas, reaction R.2 can possibly limit the NO₃ lifetime.

NO₃ can accumulate in the atmosphere at night up to several hundred ppt (as observed in the present study), usually much higher than OH. Because of these elevated mixing ratios and its high reactivity, NO₃ can react rapidly with alkenes (5, 4). In addition, NO₃ is an important oxidant of phenolic aromatic hydrocarbons such as traffic-emitted cresols because their reaction rate constants with NO₃ are comparable to their reaction rates with OH.

NO₃ can react with NO₂ and establish equilibrium with N₂O₅ (7)



Reaction R.3 is reversible due to the thermal decomposition of N₂O₅, yielding a highly temperature dependent but rapidly achieved equilibrium between NO₃, NO₂, and N₂O₅. N₂O₅ can be subsequently removed either by homogeneous or heterogeneous hydrolysis (i.e., reaction of N₂O₅ on or within aerosol particles) to produce nitric acid (6, 8)



leading to a net indirect loss of NO₃ from the atmosphere.

The removal of N₂O₅ is governed by heterogeneous chemistry and depends strongly on the aerosol composition (9). The uptake coefficient (γ) for (R.4) varies from 0.02 for uptake onto NaNO₃ aerosol (10) to over 0.1 for uptake onto H₂SO₄ aerosol (11). The first-order loss rate of N₂O₅ onto the surface of aerosols, K_{het} is given by

$$K_{\text{het}} = \frac{\gamma A \langle c \rangle}{4} \quad (2)$$

where A is the aerosol surface area, γ the reactive uptake coefficient, and <c> is the mean thermal velocity.

The present paper reports the results of a long-term (25 months) measurement campaign of the nitrate radical and other atmospheric species in Jerusalem, a continental urban semiarid area. To the best of our knowledge, no long-term observations of atmospheric nitrate chemistry have been reported for urban areas or dry desert locations with elevated levels of photochemical air pollution, together with the presence of high levels of natural and anthropogenic airborne particles. This study offers the first opportunity to investigate the statistical characteristics of the seasonal and spatial

* Corresponding author phone: +972-2-6584827; fax: +972-2-5637260; e-mail: davidasaf2@gmail.com.

patterns of NO₃ chemical characteristics under elevated mixing ratios and also to examine the controlling factors in this urban boundary layer. The mean contribution and the monthly variations of the different sink mechanisms of NO₃ were studied. In addition, a one-dimensional model was utilized to explain and reproduce the observed elevated NO₃ levels.

2. Location and Experimental Details and Methods

2.1. Experimental Setup. An air quality monitoring station was established in the urban center of Jerusalem (31°47' N 35°13' E) at the Hebrew University (HUJI), 760 m above sea level, and operated for more than two years (July 2005–September 2007). NO₃ and NO₂ were measured using LP-DOAS, long-path differential optical absorption spectroscopy (1).

The 3.8 km light path passed over several roads including a major traffic artery. The DOAS instrument, the site, and the raw data processing procedure have been described in detail in a previous paper (12). NO₃ concentrations were obtained from the spectra using an evaluation procedure described previously (13) and summarized in the Supporting Information.

Point measurements of O₃, NO/NO_x, and meteorological parameters were conducted continuously at HUJI using conventional analyzers, representing point parameters at the measuring site. Details are reported in the Supporting Information. A total of 609 nights of continuous nitrate radical measurements were conducted. No data was available for days with poor visibility, which occurred mainly during winter and autumn. On 407 nights during the study, NO₃ levels were above the detection limit of the instrument (8.5 ppt).

2.2. Model Description. Simulations were performed using a one-dimensional Chemical Transport Model, UAHCTM_1D (14). The model and its adaptation for the present study is described briefly; more detailed information is given elsewhere (15). The model includes an explicit gas-phase mechanism, which accounts for photochemical and temperature and pressure-dependent reactions. The model takes into account the vertical motion of the different species based on diffusion, advection, and deposition velocities.

Photochemistry was described by 167 gas-phase and 23 photochemical reactions, based on the Trainer mechanism (16, 17), and has been updated according to Atkinson (7). Heterogeneous removal of N₂O₅ was included in the model using parametrization for the first-order rate constant of reaction R.4, according to eq 2.

All model simulations presented here relate to November 25, 2006. Calculations of $\gamma(\text{N}_2\text{O}_5)$ averaged 0.013 for the modeled date, accounting for variations in relative humidity and temperature according to laboratory measurements (18). The total aerosol surface area, assuming constant aerosol composition (section 3.5), was estimated for the current conditions at $1.5 \times 10^{-5} \text{ (cm}^2\text{)/(cm}^3\text{)}$ (see the sensitivity analysis in the Supporting Information). All reactions that significantly influence the production and loss processes of the nitrate radical are presented in Table S1 of the Supporting Information.

Horizontal fluxes were added at heights between ground level and the base of the planetary boundary layer. Fluxes for NO and NO₂ were included on the basis of actual measurements, while fluxes for several VOCs were based on average representative urban VOC concentrations (section 3.5). Extensive sensitivity analysis was performed in order to investigate the impact of the hydrocarbons on the balance between ozone and nitrogen oxides and loss processes of the nitrate radicals. This ensured that the hydrocarbon concentrations were adequately included in the model in order to reach the goals of the study (Supporting Information).

Necessary meteorological parameters (e.g., boundary layer height and friction velocities) were obtained by running a

one-dimensional meteorological prognostic model (19), which simulated the full diurnal cycle of the boundary layer behavior for the specified day. The meteorological conditions, fluxes, solar data, and heterogeneous parametrizations were updated every 15 min in all simulations.

3. Results and Discussion

The average nighttime concentration of NO₃ for the entire campaign was 27.3 ± 43.5 pptv, 3 times higher than reported values from other long-term campaigns (2, 3, 20, 21).

NO₃ concentrations were highest during the summer seasons (Figure S1 of the Supporting Information), in agreement with previous studies (6, 18, 21). The maximum NO₃ mixing ratios (>800 pptv, July 2007) were higher than previously reported for other urban locations (Riverside, California, peaking at 288 pptv (22), and Houston, Texas aircraft measurements (23), nearly up to 400 pptv). The extreme NO₃ concentrations as observed in the present study have been reported previously (13).

As was to be expected, no dependence on wind direction was observed for NO₃ because of its short lifetime of only several minutes. The contribution from transport as compared to local production should therefore be negligible.

3.1.1. Diurnal Data Analysis. The diurnal results of half hourly averages for autumn (September–November), winter (December–February), spring (March–May), and summer (June–August) are presented in Figure 1 for the NO₃ radical and NO₂ and O₃ measurements and are averaged for the entire nighttime measurements of the campaign.

Mixing Ratios of NO₃. Autumn and spring show a similar diurnal pattern with a gradual rise in NO₃ from sunset until approximately 22:00, with average concentrations up to 20 pptv for autumn and 30 pptv for spring. The levels then remain stable with minor fluctuations until 02:00, when concentrations once more increase to mean maxima of 33 pptv at 04:30 for autumn and 43 pptv at 05:30 for spring, probably due to the rise in O₃ levels. NO₃ concentrations then remained relatively stable until sunrise, when they decrease drastically to zero levels due to rapid photolysis and the morning rush hour elevated NO emissions (reaction R.2).

During winter, mean levels rose continuously from sunset up to a mean maximum of 52 pptv at around 03:00, followed by a gradual decrease to 40 pptv before final decrease at sunrise. During summer, the mean NO₃ pattern showed a constant rise from sunset until sunrise, with mean maxima of 65.8 pptv at 05:00. The highest measured NO₃ for the entire campaign occurred during summer, with a value of 807 ppt occurring at 03:30.

Mixing Ratios of O₃ and NO₂. Ozone and NO₂ mirrored each other during nighttime for all four seasons, with ozone following, more or less, the NO₃ profile. During the evening hours, after sunset, titration of O₃ occurred by NO, producing NO₂ and hence allowing NO₃ production. The O₃ levels decreased in the evening reaching minimum values at around 20:00–21:00, followed by a rise of 10–15 ppbv, allowing further NO₃ production, and yielding significant NO₃ concentrations. This unusual rise in O₃ occurred during all four seasons, usually accompanied with a decrease in relative humidity by at least 10%, and observed frequently in Jerusalem and other Israeli cities (24). As previously proposed by Asaf, et al. (12), the most likely explanation for the ozone increase is a persisting low-level inversion trapping the daytime ozone. With the gradual lowering of the inversion layer during nighttime, the ozone level increased, peaking between 03:00 and 05:00. The highest mean nighttime O₃ concentrations occurred throughout spring and summer with levels up to 37 ppbv at around 03:00–04:00, while during winter a maximum of 33 ppbv occurred during the same time period.

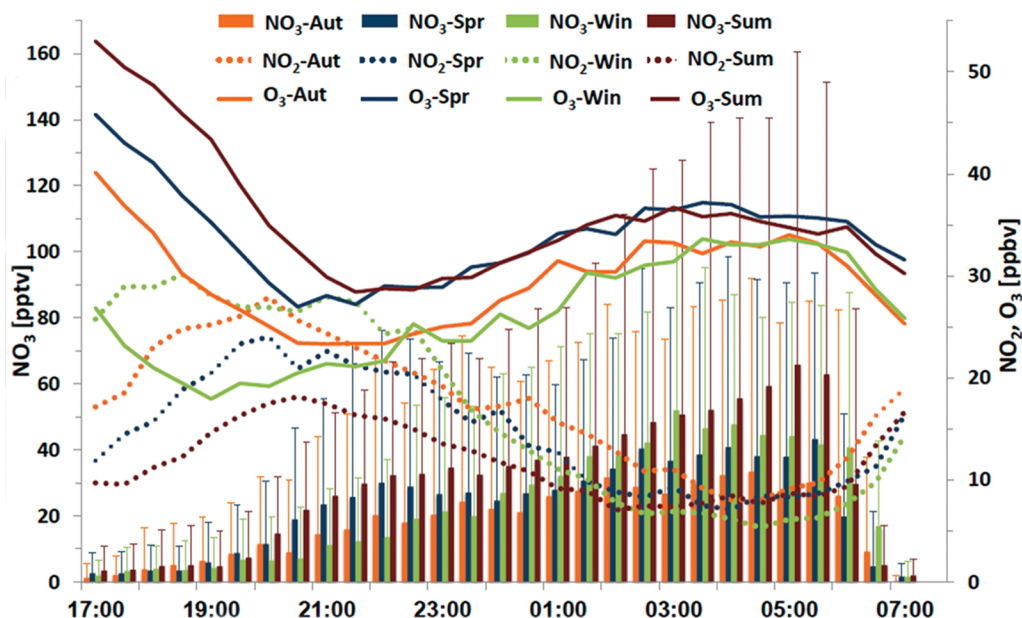


FIGURE 1. Seasonal half-hourly average concentrations of NO_3 (error bars showing SD), NO_2 , and O_3 at Jerusalem (July 2005–September 2007). NO_3 was higher and peaked later in the summer than in the winter.

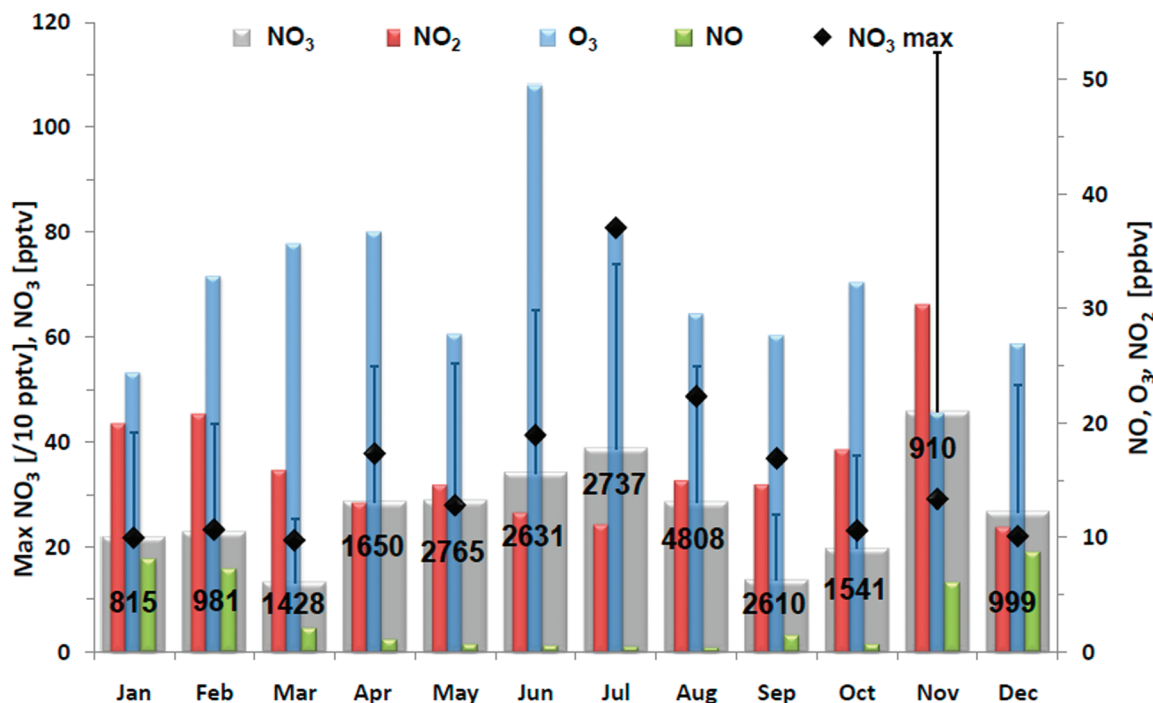


FIGURE 2. Average nocturnal monthly mixing ratios, with number of measurements from the whole campaign of NO_3 (error bars showing SD), and maximum values divided by 10 per month (left axis). In addition, average NO_2 , NO , and O_3 (right axis) are presented. Higher mean NO_3 and ozone levels in summer months, when NO levels are lower and temperatures are higher. Monthly average trends agree with the diurnal time series.

Unlike ozone, the NO_2 profile did not follow the NO_3 profile, in contrast with other studies (9, 25, 26) which reported seasonal and diurnal similarities between the NO_2 and NO_3 profiles. During the evening hours, elevated NO_2 levels corresponded to peak traffic hours, with the lowest average NO_2 levels up to 18 ppbv during summer. Winter demonstrated the highest mean with 30 ppbv due to frequent stable conditions, while autumn and spring had maximum levels of 27 and 24 ppbv, respectively. From approximately 20:00, mean NO_2 levels gradually decreased to 5–10 ppbv between 02:00–04:00, depending on the season. Because of the abundance in NO_2 in Jerusalem, there was no deficiency

in NO_3 precursors, and the NO_3 profiles were therefore not affected directly by variations in NO_2 .

A comparison with weekend measurements showed that NO_3 concentrations were 30% higher during weekdays. This analysis and detailed meteorological data can be found in the Supporting Information.

3.2. Monthly Mean Analysis. The nighttime monthly and seasonal means for NO_3 , NO_2 , NO , and O_3 and maximum mixing ratios for NO_3 are presented in Figure 2 and Table S2 of the Supporting Information. Only the nocturnal measurements are presented because NO_3 daytime measured concentrations were below the detection limits. NO_3 follows a

distinct seasonal dependency with the highest mean values during the summer months (33 ± 55 pptv). Spring mean levels were a third lower than the summer average (25 ± 38 pptv), while autumn and winter months demonstrated the lowest mean concentrations (21 ± 36 and 23.3 ± 33 pptv, respectively). The lowest mean NO_3 levels of 13.5 ± 24 pptv were reported for March. Vrekoussis et al. (20) reported similar NO_3 trends for the marine boundary layer over the East Mediterranean. The monthly peak NO_3 values ranged from a low of 214 ppt during March up to 807 ppt for July. Elevated NO_3 levels were observed especially during the warmer and dryer months. Nevertheless, Figures 2 and S1 of the Supporting Information demonstrate that elevated NO_3 levels occurred throughout the different months of the year, albeit with lowest frequency in the winter months. The elevated average value observed for November is probably due to a combination of long NO_3 lifetimes, as a consequence of reduced loss processes and elevated NO_2 concentrations.

The NO_2 levels ranged from below detection limits (0.8 ppb) to a high of 121.3 ppbv (May). The highest monthly average concentrations were observed in November (30.3 ± 24.5 ppbv) and during the winter months (17.0 ± 16.0 ppbv). The lowest average concentrations were for spring (14.5 ± 14.3 ppbv) and summer (13.0 ± 10.7 ppbv) as opposed to NO_3 , which had the highest average concentrations for those seasons.

The highest average values of NO (8.4 ± 18 ppbv) were observed between November and February, thus preventing a buildup of NO_3 concentrations and also reducing the O_3 concentrations. Considerably lower mean values were measured in the spring (1.2 ± 3.6 ppbv) and autumn (2.3 ± 2.5 ppb) months, with summer having the lowest levels of 0.4 ± 0.9 ppb. Therefore, even though the site was an urban location adjacent to major arteries, the NO levels throughout most of the year were lower than anticipated.

Nocturnal O_3 showed a similar pattern to NO_3 , peaking during July (89 ppbv). The highest average concentrations were during summer (34.7 ± 11.4 ppbv) and spring (33.9 ± 10.7 ppbv) months, while autumn (27.0 ± 10.3 ppbv) and winter (27.6 ± 11.2 ppbv) showed lower values. The monthly average trends agree with the diurnal time series trends as described earlier, supporting the notion that it is O_3 that affects the NO_3 nighttime profile under urban polluted conditions rather than NO_2 .

3.3. Statistical Regression Analysis between $[\text{NO}_3]$ and $[\text{NO}_2]$, $[\text{O}_3]$, RH, and Temperature. The relationship between the $[\text{NO}_3]$ and $[\text{NO}_2]$, $[\text{O}_3]$, RH, wind speed, and temperature were evaluated through single and multiple statistical regression models (MATLAB). The single regression analysis is detailed in the Supporting Information.

A stepwise multiple regression analysis was calibrated using half of the data set and validated with the other half ($N = 7310$ for the entire set). All the variables from the single regression analysis, except wind speed, were included in the multiple regression. O_3 and NO_2 were included separately because they were not intercorrelated ($R = -0.33$). Outlier values (less than 1% of the data) were omitted from the regression. The regression yielded the following linear correlation ($\text{adj-}R^2 = 0.13$)

$$[\text{NO}_3] = (1.84 \pm 0.02)10^{-4} \times (\text{NO}_2) + (0.88 \pm 0.01)10^{-4} \times (\text{O}_3) + (0.30 \pm 0.03) \times T + (-0.60 \pm 0.00) \times \text{RH} + (-19.8 \pm 1) \quad (3)$$

where $[\text{NO}_3]$, $[\text{NO}_2]$, and $[\text{O}_3]$ are in ppt, T in K, and RH in %. This regression had the highest $\text{adj-}R^2$ of all the regressions tested. The regression coefficients, shown together with their respective standard-errors, were significant at a confidence level of at least 97%. The results show that $[\text{NO}_3]$ is most sensitive to changes in RH, followed by temperature, and

least sensitive to changes in $[\text{NO}_2]$ and $[\text{O}_3]$. The four variables from eq 3 explain only 13.2% of the NO_3 variability, most likely due to the influence of other species and factors that were not measured in the present study and therefore not included in this analysis. The validation of eq 3 was examined for the measured versus calculated $[\text{NO}_3]$. A similar $\text{adj-}R^2 = 0.11$ was obtained.

The parameter with the highest coefficient of determination was RH, in contrast to the Finokalia campaign (20), where a similar regression found that temperature had the highest coefficient. The above study found that the correlation ($R^2 = 0.072$) was smaller compared to the present study and no correlation was found with NO_2 (20). Nevertheless, the resulting overall pattern was similar, with a positive correlation for O_3 and T and negative for RH. Because of the importance of RH, it appears that the heterogeneous removal processes have a significant role on NO_3 concentrations (section 3.5).

3.4. NO_3 Production and Degradation Rates. The annual mean rate of production of NO_3 was calculated (eq 1) to be $P_{\text{NO}_3} = 4.7 \times 10^6$ (molec)/($\text{cm}^3 \text{ s}^{-1}$).

Throughout the campaign, P_{NO_3} varied between $6 \times 10^5 - 3.8 \times 10^7$ (molec)/($\text{cm}^3 \text{ s}^{-1}$), with highest values during the sunset and early evening hours. This value was slightly higher than that reported for the Rugen long-term rural campaign (3) and an order of a magnitude higher than that reported for the Finokalia (20) and Lindenberg (2) long-term rural campaigns. The seasonal distribution of P_{NO_3} in Jerusalem showed lowest values during November–March and values twice as high during the summer months (Figure S2 of the Supporting Information) due mainly to higher temperatures and higher O_3 mixing ratios.

The total degradation frequency of NO_3 (f_{NO_3}), was calculated via eq 4 for steady state conditions

$$f_{\text{NO}_3} = \frac{[\text{NO}_2][\text{NO}_3]k_1}{[\text{NO}_3]} = \frac{1}{\tau(\text{NO}_3)} \quad (4)$$

and ranged between 1.4×10^{-4} and 0.17 s^{-1} with an annual mean of 0.01 s^{-1} and showed a reverse trend to $[\text{NO}_3]$. Additionally, during September and October a very efficient loss of NO_3 was observed (0.013 and 0.016 s^{-1} , respectively), significantly decreasing the NO_3 lifetimes and concentrations. In contrast, during November, long lifetimes (20 min) and small degradation frequencies ($1.7 \times 10^{-3} \text{ s}^{-1}$) led to higher NO_3 concentrations.

3.5. NO_3 Lifetime and Removal Paths. The NO_3 lifetime ($\tau(\text{NO}_3)$) was calculated for the entire campaign (Figure S2 of the Supporting Information). Excluding the sunrise and sunset time periods and the bursts of NO and high variability episodes of NO_2 and NO_3 , an approximate steady state is obtained because production and losses were balanced. This could have been achieved temporarily during the periods in which NO_3 lifetime and concentrations remained stable, even under high NO_x conditions (26). A thermal equilibrium was probably achieved for reaction R.3 because the thermal N_2O_5 lifetime is on the order of 20 s, while the average NO_3 lifetime is on the order of 5–20 min. Furthermore, on the basis of the K_{eq} range from this campaign and NO_2 levels of ~ 10 ppb, a value of between 10–30 is calculated for the ratio of $[\text{N}_2\text{O}_5]/[\text{NO}_3]$. Thus, if indirect losses dominate, the N_2O_5 lifetime should be at least 10 times the observed NO_3 lifetime, i.e., 50–200 minutes. This is up to 3 orders of magnitude higher than the thermal lifetime of N_2O_5 , and thus thermal equilibrium is a very good approximation.

A number of processes, either direct or indirect, can scavenge the nitrate radical during nighttime, and these can be distinguished through correlation analyses. In cases where the direct removal paths are negligible, the relative importance can be estimated through the relationship between

TABLE 1. Linear Regressions of P_{NO_3} vs $[\text{NO}_3]$ (Indicating Direct Removal) and of $\ln(\tau(\text{NO}_3))$ vs $\ln[\text{NO}_2]$ (Indicating Indirect Removal) for Each Season^a

season	direct loss indicators $[\text{NO}_3] = a \times (P_{\text{NO}_3}) + b(R^2)$	τNO_3 due to effect of direct losses (min)	indirect loss indicators $\ln(\tau(\text{NO}_3)) = -a \times \ln[\text{NO}_2] + b(R^2)$	τNO_3 due to effect of indirect losses (min)
Win_06	$y = -647.1x + 132(0.58)$	4.7	$y = -1.1x + 8.1(0.67)$	3.8
Win_07	$y = -825.1x + 170(0.43)$	24.3	$y = -0.9x + 8.0(0.64)$	17.1
Spr_06	$y = 191.7x + 20.8(0.11)$	4.3	$y = -0.49x + 6.4(0.33)$	6.7
Spr_07	$y = 211.0x + 48.5(0.14)$	3.4	$y = -0.3x + 5.4(0.06)$	15.8
Sum_05	$y = 66.1x - 58.5(0.12)$	1.2	$y = -0.5x + 6.9(0.49)$	6.9
Sum_06	$y = 207.5x - 69.4(0.14)$	3.9	$y = -0.5x + 6.8(0.42)$	8.1
Sum_07	$y = 474.3x - 68.1(0.44)$	3.2	$y = -0.5x + 6.6(0.27)$	5.0
Aut_05	$y = 145.4x - 0.5(0.36)$	1.6	$y = -0.2x + 5.2(0.02)$	5.5
Aut_06	$y = -524.1x + 149(0.25)$	29.1	$y = -0.8x + 8.7(0.44)$	20.4
Campaign	$y = 458.7x - 37.2(0.17)$	3.3	$y = -0.6x + 6.8(0.34)$	7.8

^a Lifetimes of NO_3 represent the effect of the direct and indirect loss for each season and are evaluated from the inverse steady state of NO_3 lifetimes vs $K_{\text{eq}}(T)[\text{NO}_2]$ (eq 5). $[\text{NO}_3]$ is expressed in pptv, P_{NO_3} in pptv s^{-1} , NO_2 in ppbv, and $\tau(\text{NO}_3)$ in min. The coefficient of determination, R^2 , for each regression is presented in parentheses.

$\tau(\text{NO}_3)^{-1}$ and $[\text{NO}_2]$, which should be proportional if the indirect pathways dominate (3). In cases of negligible indirect losses, P_{NO_3} is predicted to be proportional to $[\text{NO}_3]$, so a linear fit would indicate a possible importance of the direct sinks (3).

Linear regressions of P_{NO_3} versus $[\text{NO}_3]$ and of $\ln(\tau(\text{NO}_3))$ versus $\ln[\text{NO}_2]$ for the various seasons (Table 1) show a wide seasonal variability of direct vs indirect removal paths of NO_3 . A linear regression of the entire data set between P_{NO_3} and $[\text{NO}_3]$ yielded: $P_{\text{NO}_3} = 458.7[\text{NO}_3] - 37.2$, ($R^2 = 0.17$) and suggests the importance of the direct sinks. However, a polynomial correlation produced a better fit of $R^2 = 0.42$, indicating the dependency was not exclusively linear, suggesting the presence of indirect removal paths. During summer and spring, a positive linear fit was observed, suggesting dominance of the direct NO_3 losses. Because of the large variability and scatter of the observations, the slopes are associated with high uncertainties and R^2 is relatively low, although it is highly significant at the 95% confidence level.

With respect to the various pathways dominating the direct sink mechanisms, the dependence of $[\text{NO}_3]$ on $[\text{NO}]$ showed that NO acts as the most significant scavenger when it is present during the night for long time periods. Even though nocturnal NO concentrations were occasionally elevated due to local sources, the concentrations were usually near zero due to rapid titration with ozone within several minutes, together with the absence of photolytic conversion of NO_2 to NO .

The VOCs are also important as direct scavengers of NO_3 in the continental boundary layer (3, 6). Although organic compounds were not measured during the present campaign, a combined lifetime of about 180 s with NO_3 was calculated for a group of 30 major VOCs (Table S3 of the Supporting Information), including alkanes, alkenes, alkynes, and aromatics, estimated from several campaigns conducted in similar urban locations (12). The VOC concentrations chosen for these calculations have to be viewed with caution because they represent conditions typical of an urban location and not necessarily the actual conditions in Jerusalem. Rate constants of the selected VOCs were taken from Atkinson (8, 27). The estimated lifetime of NO_3 via VOC removal was compatible with the averaged measured lifetime of summer and spring (280 s) from the present study, suggesting that this seasonal trend is a contribution of VOC- NO_3 reactions, which are potentially a major NO_3 loss pathway. NO_3 concentrations demonstrated a significant correlation to P_{NO_3} for summer and spring and to a lesser extent for autumn (Table 1), indicating an influence of the direct loss processes on nitrate radical levels.

In addition to the contribution of the direct sinks, a very significant removal path for NO_3 is the indirect removal through conversion to N_2O_5 and its subsequent heterogeneous reactions. Previous studies found it to be an important removal path of NO_3 for marine (3, 20, 21) and continental (6) boundary layers. To minimize the scatter in the HUJI measurements, $\tau(\text{NO}_3)$ was averaged per unit of 0.1 ppbv NO_2 . The linear fit for the entire two year campaign yielded the indirect dependency of $\ln(\tau_{\text{NO}_3}) = -0.6 \ln[\text{NO}_2] + 6.8$ ($R^2 = 0.34$), indicating a contribution from indirect losses. Winter measurements showed the most significant indirect removal, with slopes reaching -1 ($R^2 = 0.67$). Furthermore, P_{NO_3} was not positively correlated with $[\text{NO}_3]$, suggesting a minor contribution of direct sinks.

Contribution of the indirect losses was also observed during autumn, demonstrating that even despite the abundance of NO and VOCs, the indirect removal path can be significant in the urban boundary layer. This observation is supported by model simulations (section 3.6). Long-term records show elevated concentrations of aerosols in Jerusalem, especially sulfate (average $15\text{--}20 \mu\text{g}/\text{m}^3$), with a relatively constant composition (28). Gamma variability is, therefore, expected to be very low, decreasing any possible confounding by RH and water content. An analysis of $[\text{NO}_3]$ versus RH (Figure S3a of the Supporting Information) was performed, including slopes calculated from the regression of $\ln(\tau_{\text{NO}_3})$ vs $\ln[\text{NO}_2]$ as a function of RH. As RH increases, the slopes approach -1 , indicating the higher significance of indirect losses of NO_3 . As RH decreases from 80 to 30%, the average concentrations of NO_3 increase by a factor of 3. This negative relationship is even more evident when examining $[\text{NO}_3]$ and $\tau(\text{NO}_3)$ vs H_2O mixing ratios, accounting for the temperature dependence (panels b and c of Figure S3 of the Supporting Information). This indicates that the indirect sinks via N_2O_5 become more important with increasing water vapor in the atmosphere. Because the hygroscopic growth of aerosols increases the surface available for heterogeneous reactions, the N_2O_5 uptake on aerosols could contribute substantially to the indirect removal of NO_3 and the conversion of NO_x to HNO_3 (5).

Brown et al. (26) suggested that a plot of $\tau(\text{NO}_3)^{-1}$ against $K_{\text{eq}}(T)[\text{NO}_2]$ (eq 5) should give a straight line whose slope and intercept are the effective first-order loss rate coefficients for N_2O_5 ($k_{\text{N}_2\text{O}_5}$) and NO_3 (k_{NO_3}), respectively. This analysis takes into consideration the temperature dependence. The ratio between the lifetimes can give a quantitative measure of the relative importance of each loss mechanism. The results show clear evidence of a rapid direct sink for NO_3 during most of the campaign, excluding winter and to a lesser extent autumn (Table 1).

$$\tau(\text{NO}_3) \equiv \frac{[\text{NO}_3]}{k_1[\text{O}_3][\text{NO}_2]} \approx (k_{\text{NO}_3} + K_{\text{N}_2\text{O}_5}K_{\text{eq}}(T)[\text{NO}_2])^{-1} \quad (5)$$

Indirect losses contribute less than half of the direct losses averaged over the entire campaign. In summer, the indirect effect was only 15% of the direct losses, as opposed to winter and autumn seasons (2006), where the indirect losses were more predominant as can be seen from the shorter $\tau(\text{NO}_3)$. Calculated NO_3 lifetimes, from summer and parts of spring and autumn, were close to the calculated lifetimes from reactions with typical local urban organic compounds (12), suggesting it is the VOC removal pathway that plays the major role in NO_3 loss. Further analysis of the data could not be performed due to lack of VOC measurements during the present campaign.

3.6. Model Simulations. The UAHCTM_1D model was used in an attempt to understand the detailed behavior of NO_3 , its precursors, and loss processes. On the basis of our measurements, it appeared that elevated NO_3 levels could only be explained by considering the intrusion of O_3 -rich air during the night. To examine this hypothesis, measurements from November 25, 2006, were chosen as a representative scenario demonstrating typically high NO_3 concentrations, accompanied with sharp fluctuations, apparently due to increases in O_3 and NO. Therefore, variables that were evaluated were episodes of elevated NO_3 levels, O_3 intrusion events, and NO nighttime emissions. These trends are unique to Jerusalem as compared to other urban and rural sites. The model was run under three conditions in order to investigate the influence of O_3 and NO on NO_3 . For the base case simulation ("Full"), horizontal O_3 fluxes [e.g., 1.0×10^{12} (molec)/(cm^3 s)] or the latter ozone peak were added between 20:45–03:30 in order to account for the entrainment of the nighttime O_3 (section 3.1.1), together with NO fluxes that were introduced to represent local observed emissions. Simulation "noNO" was run without NO fluxes between 20:00–05:45. For the "noNO-OZ" simulation, O_3 and NO fluxes were omitted throughout the entire night.

The "Full" simulation was successful in describing the overall trends in the measured NO_3 concentrations as can be observed in Figure 3a. For the "noNO-OZ" simulation, the NO_3 levels were about a quarter of the observed levels and remained stable throughout the night. After including the ozone flux in the model (simulation "noNO"), the simulated NO_3 increased to levels similar to the observed NO_3 . This demonstrates that the major reason for the elevated nitrate radical levels and their short-term variability is the intrusion of fresh ozone during nighttime. In addition, the decrease in the observed NO_3 levels between 00:00–04:00am could be reproduced by adding an NO flux of 2.0×10^9 (molec)/(cm^3 s) during the "Full" simulation, which led to the agreement between the simulation and the observed trends. This emphasizes the important role of (R2), the reaction of NO with NO_3 , in urban nocturnal chemistry. In addition, NO yielded lower mixing ratios during the first peak (23:00) due to the point NO measurements, which affected the simulated NO_3 levels in contrast to their measured spatial levels in the 3.8 km air mass along the light path. It is evident that this reaction has a dominant role in the fluctuations in NO_3 , as demonstrated by the "Full" simulation, which showed that the observed and simulated NO_3 decreased by more than 50% between 23:00–01:00. An important finding of the present study for an urban polluted environment is that O_3 can function as a limiting factor in the production of elevated NO_3 levels.

The model also indicates that the major loss process of NO_3 during most of this night is via N_2O_5 heterogeneous loss (Figure 3b). According to the calculations, losses via NO and VOCs played a significant role until 22:00, yielding short NO_3

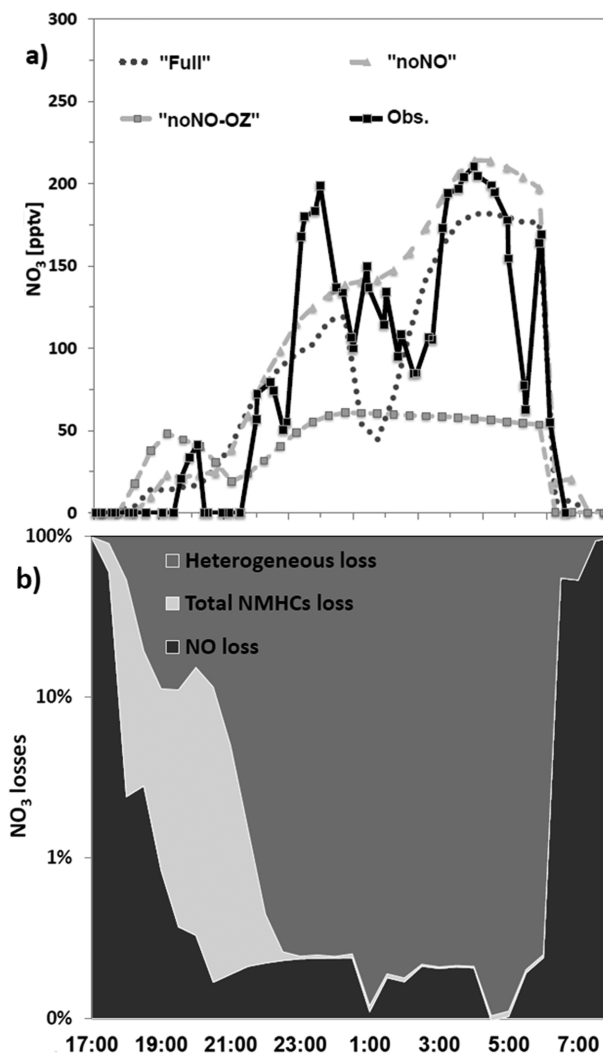


FIGURE 3. (a) Diurnal profile of observed NO_3 and the three model simulations. "Full", O_3 and NO fluxes, were included on the basis of measurements; "noNO", NO fluxes, were eliminated between 20:00–05:45; noNO-OZ-NO and O_3 fluxes were eliminated during the entire night. NO_3 trends and elevated levels were mostly influenced by changes in O_3 and NO. (b) Average loss profiles derived for the important loss mechanisms.

lifetimes between <1 –400 s. In addition, the ozone intrusion not only increased the NO_3 production but also led to NO depletion that caused the VOCs to become the dominant terminator for NO_3 rather than NO. From 22:00, the NO and VOCs presence in the boundary layer became exhausted, and the NO_3 began building up to significant levels. The major removal path then became the heterogeneous loss via N_2O_5 , yielding long nitrate radical lifetimes of 800–3000 s. At sunrise, the advected fresh NO and photolytic destruction dominated the losses, reducing the lifetimes to less than 1 s.

A linear regression of $\ln(\tau[\text{NO}_3])$ vs $\ln([\text{NO}_2])$ for 25.11.06 yielded the relationship $\ln(\tau[\text{NO}_3]) = -1.00 \times \ln([\text{NO}_2]) + 9.77$, supporting the model results. The slope of -1 implies that the dominant NO_3 loss was via indirect loss. However, because the correlation was not perfect ($R^2 = 0.7$), indirect removal of NO_3 was not the exclusive pathway. Using the analysis suggested by Brown et al. (26) indicated that the effects of direct losses contribute about 20% to the total losses.

The above results suggest several conclusions can be drawn about the NO_3 chemistry in semiarid urban areas. First, direct loss processes of NO_3 predominate in the urban atmosphere and shorten its lifetime, especially during the warmer seasons. Second, the cold seasons are dominated by

indirect N₂O₅ losses, as described by the mechanistic studies and the model simulations. Third, NO₃ trends and concentrations are most sensitive to changes in ozone and nitrogen oxide levels; and finally, the extreme high levels of NO₃ can be expected under conditions with entrainment of nighttime ozone.

Acknowledgments

Financial support for the present project was provided by the GIF Grant I-776-288/2003. We thank A. Biazar for helpful insights on atmospheric modeling and V. Roshal for insights on statistical analysis.

Supporting Information Available

Additional analyses, figures, and tables. This material is available free of charge via the Internet at <http://pubs.acs.org>.

Literature Cited

- (1) Platt, U. Differential Optical Absorption Spectroscopy (DOAS) in Air Monitoring by Spectroscopic Techniques. In *Chemical Analysis Series 127*; Sigrist, M. W., Ed.; Wiley: New York, 1994; pp 24–87.
- (2) Geyer, A.; Ackermann, R.; Dubois, R.; Lohrmann, B.; Mueller, T.; Platt, U. Long-term observation of nitrate radicals in the continental boundary layer near Berlin. *Atmos. Environ.* **2001b**, *35*, 3619–3631.
- (3) Heintz, F.; Flentje, H.; Dubois, R.; Platt, U. Long-term observation of nitrate radicals at the Tor Station, Kap Arkona (Rugen). *J. Geophys. Res.* **1996**, *101*, 22,891–22,910.
- (4) Smith, N.; Plane, J. M. C.; Nien, C. F.; Solomon, P. A. Nighttime radical chemistry in the San Joaquin Valley. *Atmos. Environ.* **1995**, *29*, 2887–2897.
- (5) Carslaw, N.; Plane, J. M.; Coe, H.; Cuevas, E. Observations of the nitrate radical in the free troposphere at Izana de Tenerife. *J. Geophys. Res.* **1997**, *102*, 10613–10622.
- (6) Geyer, A.; Alicke, B.; Konrad, S.; Schmitz, T.; Stutz, J.; Platt, U. Chemistry and oxidation capacity of the nitrate radical in the continental boundary layer near Berlin. *J. Geophys. Res.* **2001a**, *106*, 8013–8025.
- (7) Atkinson, R.; Baulch, D. L.; Cox, R. A.; Crowley, J. N.; Hampson, R. F.; Kerr, J. A.; Rossi, M. J.; Troe, J. Summary of evaluated kinetic and photochemical data for atmospheric chemistry: Volume II. Gas phase reactions of organic species. *Atmos. Chem. Phys.* **2006**, *6*, 3625–4055.
- (8) Vrekoussis, M.; Kanakidou, M.; Mihalopoulos, N.; Crutzen, P. J.; Lelieveld, J.; Perner, D.; Berresheim, H.; Baboukas, E. Role of the NO₃ radicals in oxidation processes in the eastern Mediterranean troposphere during the MINOS campaign. *Atmos. Chem. Phys.* **2004**, *4*, 169–182.
- (9) Folkers, M.; Mentel, T. F.; Wahner, A. Influence of an organic coating on the reactivity of aqueous aerosols probed by the heterogeneous hydrolysis of N₂O₅. *Geophys. Res. Lett.* **2003**, *30* (12), 1644–1648.
- (10) Mentel, T. F.; Sohn, M.; Wahner, A. Nitrate effect in the heterogeneous hydrolysis of dinitrogen pentoxide on aqueous aerosols. *Phys. Chem. Chem. Phys.* **1999**, *1*, 5451–5457.
- (11) Hanson, D. R.; Ravishankara, A. R. The reaction probabilities of ClONO₂ and N₂O₅ on 40 to 75 percent sulfuric acid solutions. *J. Geophys. Res.* **1991**, *96* (D9), 17307–17314.
- (12) Asaf, D.; Pedersen, D.; Matveev, V.; Peleg, M.; Kern, C.; Zingler, J.; Platt, U.; Luria, M. Long-term measurements of NO₃ radical at a semiarid urban site: 1. Extreme concentration events and their oxidation capacity. *Environ. Sci. Technol.* **2009**, *43*, 9117–9123.
- (13) Matveev, V.; Luria, M.; Alper, D.; Peleg, M. Long-range transportation of air pollutants from Europe towards Israel. *Isr. J. Earth Sci.* **2002**, *51*, 17–28.
- (14) Biazar, A. P. The Role of Natural Nitrogen Oxides in Ozone Production in the Southern Environment. Dissertation, The University of Alabama in Huntsville, Huntsville, AL, 1995.
- (15) Tas, E.; Peleg, M.; Pedersen, D. U.; Matveev, V.; Biazar, A. P.; Luria, M. Measurement-based modeling of bromine chemistry in the boundary layer: 1. Bromine chemistry at the Dead Sea. *Atmos. Chem. Phys.* **2006**, *6*, 5589–560.
- (16) Trainer, M.; Hsie, E. Y.; Mackeen, S. A.; Tallamraju, R.; Parrish, D. D.; Fehsenfeld, F. C.; Liu, S. C. Impact of natural hydrocarbons on hydroxyl and peroxy radicals at remote site. *J. Geophys. Res.* **1987**, *92*, 11879–11894.
- (17) Trainer, M.; Buhr, M. P.; Curran, C. M.; Fehsenfeld, F. C.; Hsie, E. Y.; Liu, S. C.; Norton, R. B.; Parrish, D. D.; Williams, E. J. Observations and modeling of the reactive nitrogen photochemistry at a rural site. *J. Geophys. Res.* **1991**, *96*, 3045–3063.
- (18) Kane, S. M.; Caloz, F.; Leu, M. T. Heterogeneous uptake of gaseous N₂O₅ by (NH₄)₂SO₄, NH₄HSO₄, and H₂SO₄ aerosols. *J. Phys. Chem. A* **2001**, *105*, 6465–6470.
- (19) McNider, R. T.; Pielke, R. A. Diurnal boundary-layer development over sloping terrain. *J. Atmos. Sci.* **1981**, *38*, 2198–2212.
- (20) Vrekoussis, M.; Mihalopoulos, N.; Gerasopoulos, E.; Kanakidou, M.; Crutzen, P. J.; Lelieveld, J. Two years of NO₃ radical observations in the boundary layer over the Eastern Mediterranean. *Atmos. Chem. Phys.* **2007**, *7*, 315–327.
- (21) Allan, B. J.; Carslaw, H.; Coe, R.; Burgess, A.; Plane, J. C. Observations of the nitrate radical in the marine boundary layer. *Atmos. Chem. Phys.* **1999**, *33*, 129–154.
- (22) Platt, U.; Perner, D.; Potz, H. Simultaneous measurement of atmospheric CH₂O, O₃, and NO₂ by differential optical absorption. *J. Geophys. Res.* **1979**, *84*, 6329–6335.
- (23) Brown, S. S.; Dube, W. P.; Fuchs, H.; Ryerson, T. B.; Wollny, A. G.; Brock, C. A.; Bahreini, R.; Middlebrook, A. M.; Neumna, J. A.; Atlas, E.; Roberts, J. M.; Osthoff, H. D.; Trainer, M.; Fehsenfeld, F. C.; Ravishankara, A. R. Reactive uptake coefficients for N₂O₅ determined from aircraft measurements during the second Texas Air Quality study: Comparison to current model parameterizations. *J. Geophys. Res.* **2009**, *114*, D00F10.
- (24) Steinberger, E. H.; Ganor, E. High ozone concentrations at night in Jerusalem and Tel-Aviv. *Atmos. Environ.* **1980**, *14* (2), 221–225.
- (25) Allan, B. J.; McFiggans, G.; Plane, J. M.; Coe, H.; McFadyen, G. G. The nitrate radical in the remote marine boundary layer. *J. Geophys. Res.* **2000**, *105*, 24191–24204.
- (26) Brown, S. S.; Stark, H.; Ravishankara, A. R. Applicability of the steady state approximation to the interpretation of atmospheric observations of NO₃ and N₂O₅. *J. Geophys. Res.* **2003**, *108*, 4539–4546.
- (27) Atkinson, R. Gas-phase tropospheric chemistry of volatile organic compounds. I. Alkanes and alkenes. *J. Phys. Chem. Ref. Data.* **1997**, *26*, 215–290.
- (28) Foner, H. A.; Ganor, E. The chemical and mineralogical composition of some urban atmospheric aerosols in Israel. *Atmos. Environ.* **1992**, *26B*, 125–133.

ES100967Z